Simultaneous Measurement of Complementary Observables with Compressive Sensing

Gregory A. Howland,[1*] James Schneeloch, Daniel J. Lum, and John C. Howell
Department of Physics and Astronomy, University of Rochester, 500 Wilson Boulevard, Rochester, New York 14618, USA
(Received 18 March 2014; published 26 June 2014)

The more information a measurement provides about a quantum system's position statistics, the less information a subsequent measurement can provide about the system's momentum statistics. This information trade-off is embodied in the entropic formulation of the uncertainty principle. Traditionally, uncertainly relations correspond to resolution limits; increasing a detector's position sensitivity decreases its momentum sensitivity and vice versa. However, this is not required in general; for example, position information can instead be extracted at the cost of noise in momentum. Using random, partial projections in position followed by strong measurements in momentum, we efficiently determine the transverse-position and transverse-momentum distributions of an unknown optical field with a single set of measurements. The momentum distribution is directly imaged, while the position distribution is recovered using compressive sensing. At no point do we violate uncertainty relations; rather, we economize the use of information we obtain.

DOI: 10.1103/PhysRevLett.112.253602 PACS numbers: 42.50.Xa, 03.65.Ta, 03.65.Wj, 89.70.Cf

Measurements on quantum systems are always constrained by uncertainty relations. Localizing a particle in one observable, such as position, imparts a disturbance that makes a following measurement of a complementary observable, such as momentum, unpredictable. Such *strong*, projective measurements are often said to "collapse" the quantum wave function. For example, in Young's double slit experiment, it is not possible to detect through which slit particles pass (position) while also observing interference fringes in the far field (momentum) [1].

Consequently, the statistics of complementary observables are usually measured separately; an ensemble of identically prepared particles is directed to a position detector and a different, similarly prepared ensemble is directed to a momentum detector. If a detector instead measures both observables simultaneously with strong measurements, its position resolution Δ_x and momentum resolution Δ_k are bounded by Heisenberg's uncertainty relation, $\Delta_x\Delta_k \geq 1/2$. In its most basic form, a Shack-Hartmann wave-front sensor is an example of this kind of detector [2].

Though this resolution limitation applies to strong measurements, it is not true in general. Here, the uncertainty principle implies an information exclusion principle [3,4]; the more information a detector gives about position, the less information it can provide about momentum and vice versa. With a single, carefully designed experiment, one can simultaneously recover the statistics of both observables at arbitrary resolution. This has been demonstrated, albeit very inefficiently, with weak measurement [5–7].

In this Letter, we efficiently obtain the transverse-position and transverse-momentum distributions of optical photons from a single set of measurements at high resolution. We sequentially perform a series of random, partial projections in position followed by strong projective measurements of the momentum. The partial projections efficiently extract information about the photons' position distribution at the cost of injecting a small amount of noise into their momentum distribution. This allows the momentum distribution to be directly observed on a charge-coupled device (CCD) camera. The position distribution is recovered using a computational technique called compressive sensing (CS) [8].

Consider an optical field in the plane $z = z_0$ with transverse, complex amplitude $\psi(\vec{x})$, where z is the propagation direction and $\vec{x} = (x, y)$ are transverse, spatial coordinates. The field also has momentum amplitude $\psi(\vec{k})$, which is related to $\psi(\vec{x})$ by a Fourier transform, with $\vec{k} = (k_x, k_y)$.

To measure the position field intensity $|\psi(\vec{x})|^2$, one could raster scan a small pinhole through the transverse plane at $z = z_0$. The fractional power passing through the pinhole as a function of its position reveals the image. From a quantum perspective, this process constitutes a *strong* projective position measurement; the pinhole localizes the position of photons passing through it and their subsequent momenta are random. From a classical optics perspective, the pinhole acts like a spatial filter; light passing through the pinhole diffracts evenly in all directions. In either case, information about the original field's momentum $\psi(\vec{k})$ is lost. Note that one could instead choose to measure the momentum distribution $|\psi(\vec{k})|^2$ by performing a similar scan in the focal plane of a Fourier transforming lens. Here, position information would instead be forfeit.

In our approach (Fig. 1), we perform a series of partially projective measurements of position followed by strong measurements of momentum. We first prepare a transverse, photonic state $\psi(\vec{x})$ by illuminating an object mask with a

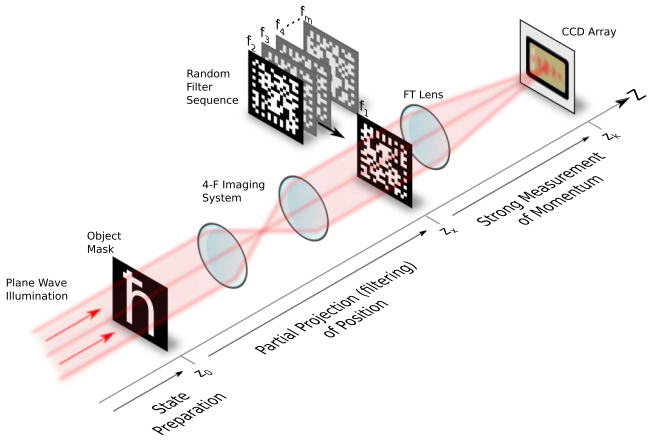

FIG. 1 (color online). Experimental setup for simultaneous position and momentum imaging. A state is prepared by illuminating an object mask at $z = z_0$ with a plane wave from an attenuated HeNe laser. The field is imaged at $z = z_x$ where it is sequentially filtered by a series of M 256 × 256-pixel, random binary filters $\boldsymbol{F_i}$. Each filter partially projects the state by blocking about half of the position elements. A cooled CCD array in the focal plane $z = z_k$ of a Fourier-transforming lens records the momentum distribution for each filtered state. Position information is mapped to the total optical power passing each filter; this measures the correlation between the position intensity distribution at z_x with the current filter. Because the filters do not strongly localize the photons' position, the momentum distribution is directly recovered by averaging the CCD images. The position distribution is reconstructed using compressive sensing techniques such that an N-pixel position image requires $M \ll N$ filters.

collimated laser. We image this field in the plane $z = z_x$ with a 4f imaging system. Here we sequentially perform partial projections of $\psi(\vec{x})$ by filtering it with a series of M binary amplitude masks $f_i(\vec{x})$. Each mask consists of a random, N-pixel pattern, where each pixel either fully transmits or fully obstructs with equal probability. Note that the total optical power passing the ith filter gives the correlation between that filter and the position intensity distribution $|\psi(\vec{x})|^2$. In this way, a small amount of information about the position distribution is extracted without localizing the field. The filtered state $\tilde{\psi}_i(\vec{x}) = \psi(\vec{x}) f_i(\vec{x})$ then passes through a Fourier transforming lens to a CCD array in the lens' focal plane at $z = z_k$. The CCD records M images of the momentum distribution of the filtered field $|\tilde{\psi}_i(\vec{k})|^2$, one for each filter. This set of images contains information about both ψ's position and momentum.

The momentum distribution is recovered directly from the CCD images $|\tilde{\psi}(\vec{k})|^2$ by simple averaging such that

$$|\psi(\vec{k})|^2 = \langle |\tilde{\psi}_i(\vec{k})|^2 \rangle, \tag{1}$$

where angled brackets indicate an average over all filters. This is made possible by the surprising fact that $|\tilde{\psi}_i(\vec{k})|^2$ is a good approximation to $|\psi(\vec{k})|^2$, even though $|\tilde{\psi}_i(\vec{x})|^2$ is missing half of its coefficients.

By the convolution theorem of Fourier optics [9], the filtered ith momentum distribution is found by convolving the Fourier transforms of $\psi(\vec{x})$ and $f_i(\vec{x})$ such that

$$|\tilde{\psi}_i(\vec{k})|^2 = |\psi(\vec{k}) \otimes f_i(\vec{k})|^2, \tag{2}$$

where $\otimes$ denotes convolution. To understand the filter's effect on $\psi(\vec{k})$, we must consider its Fourier transform (Fig. 2).

At high resolution, each transmitting filter pixel is approximately a displaced Dirac delta function [Fig. 2(a)] with unit amplitude. The Fourier transform of each delta function is a plane wave propagating at an angle proportional to its displacement from the origin. At $\vec{k} = (0, 0)$, these plane waves add in phase, producing a sharp peak. For $\vec{k} \neq (0, 0)$, each plane wave is equally likely to provide a negative or positive contribution. The coefficients therefore follow a random, complex Gaussian distribution [10]. A filter's Fourier transform is approximately a Dirac delta function at zero momentum riding a small noise floor that is a factor $\sqrt{2/N}$ weaker [Fig. 2(b)],

$$f_i(\vec{k}) \propto \delta(\vec{k}) + \sqrt{\frac{2}{N}} \phi_i(\vec{k}). \tag{3}$$

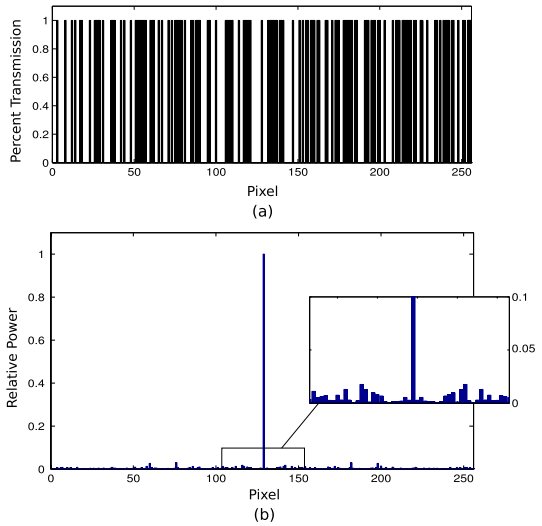

FIG. 2 (color online). Discrete Fourier transform of a 256-pixel, one-dimensional random binary pattern. Panel (a) gives a random, binary one-dimensional filter function where a value 1 is fully transmitting and a value 0 is fully obstructing. Panel (b) shows the relative power spectrum of its Fourier transform, where the zero-momentum term is scaled to unity. The noise floor is a factor $\sqrt{2/N}$ weaker in amplitude in both its mean and standard deviation. The same relationship holds for a two-dimensional filter.

Values for $\phi_i(\vec{k})$ follow a random, complex Gaussian white noise distribution, with real and imaginary parts of zero mean and standard deviation $1/\sqrt{2}$.

Because a convolution with a delta function simply returns the original function, we expect $\tilde{\psi}_i(\vec{k}) \approx \psi(\vec{k})$ with a small amount of noise (Fig. 3). From Eqs. (2) and (3), we find

$$|\tilde{\psi}_i(\vec{k})|^2 = \mathcal{N}\left\{|\psi(\vec{k})|^2 + \frac{2\sqrt{2}}{\sqrt{N}}\mathrm{Re}[\psi^*(\vec{k})(\psi(\vec{k}) * \phi_i(\vec{k}))] + \frac{2}{N}|\psi(\vec{k}) * \phi_i(\vec{k})|^2\right\}, \quad (4)$$

where $\mathcal{N}$ is a normalizing constant. The first term is the desired outcome; the following two terms add noise. For large N, these terms vanish. In the worst case, the signal-to-noise ratio scales as $\sqrt{N}$. At typical imaging resolutions—such as $N = 256 \times 256$ pixels used in this Letter—these terms are weak. When averaged over many patterns, the second term vanishes and the third term approaches a very small constant value. Equation (1) is therefore recovered up to a constant offset. The noiseless case is asymptotically approached for increasing M and N. Rigorous derivation of Eqs. (3,4) can be found in the Supplemental Material [11]. This analysis is closely related to similar problems in wireless communication [12].

Because the filtered momentum distribution is only lightly perturbed, very little information about the position distribution can be extracted from each CCD image. To maximize the usefulness of this information, we turn to

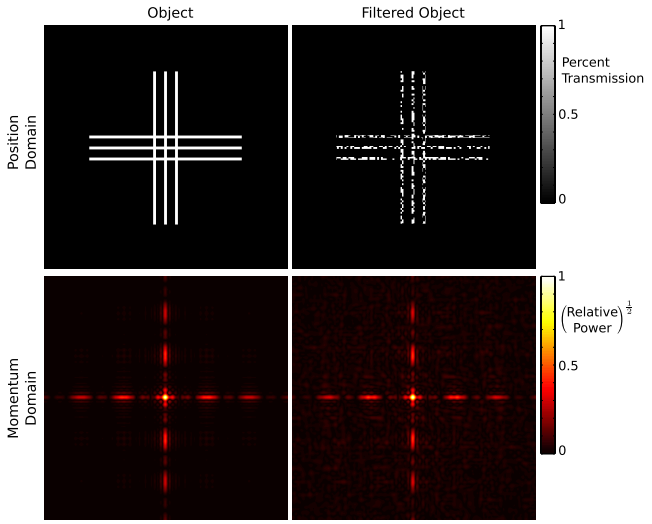

FIG. 3 (color online). Partial projections of $\boldsymbol{\psi}$. The figure simulates the effect of filtering a triple slit object with a 128×128-pixel random binary pattern. The momentum images are given as relative powers, where their maximum value is scaled to unity. A square-root color mapping emphasizes weaker momentum values. The filtered momentum distribution is a slightly noisy version of the true momentum distribution.

compressive sensing [13–15]. Compressive sensing [8] is an extremely efficient measurement technique for recovering an N-dimensional signal from $M \ll N$ measurements, provided the signal can be compressed in a known way. The use of outside information—the prior knowledge that a signal is compressible—is a powerful tool for economizing measurement. In the past decade, compressive sensing has taken the signal processing world by storm with applications ranging from magnetic resonance imaging [16] to radio astronomy [17]. More recently, CS has made inroads into the quantum domain with compressive tomography [18–20] and entanglement characterization [21]. When used for imaging, compressive sensing is closely related to computational imaging [22,23].

Together, the filters and CCD implement a single-pixel camera for the position distribution. The single-pixel camera is the textbook example of compressive sensing and has been extensively investigated [14,24]. Consider the total power Y_i striking the CCD while filtering with f_i, obtained by integrating the ith momentum image $|\tilde{\psi}_i(\vec{k})|^2$ over all CCD pixels. The CCD now acts as a single-element power meter. The value Y_i is a correlation between the position intensity $|\psi(\vec{x})|^2$ and the ith filter.

These correlations are concisely represented by the series of linear equations

$$\boldsymbol{Y} = \boldsymbol{F}\boldsymbol{X}. \quad (5)$$

Here, $\boldsymbol{F}$ is an $M \times N$ sensing matrix whose ith row is a one-dimensional reshaping of the ith filter function. $\boldsymbol{X}$ is an N-dimensional vector representing a one-dimensional reshaping of the unknown position distribution $|\psi(\vec{x})|^2$, discretized to the same resolution as the filters.

The correlations can be used to iteratively recover $\boldsymbol{X}$ by taking a weighted sum of the filter functions,

$$\boldsymbol{X} = \frac{1}{M}\sum_{i=1}^{M} \boldsymbol{Y}_i \boldsymbol{F}_i, \quad (6)$$

but many measurements are required ($M \geq N$) [25]. Instead, given some reasonable assumptions, compressive sensing dramatically reduces the requisite number of measurements ($M \ll N$).

When $M \ll N$, Eq. (5) is underdetermined; there are many possible $\boldsymbol{X}$ consistent with $\boldsymbol{Y}$. CS posits that the correct $\boldsymbol{X}$ is the one which is sparsest (has the fewest number of nonzero elements) in a representation where $\boldsymbol{X}$ is compressible. This $\boldsymbol{X}$ is found by solving the regularized least-squares optimization problem

$$\min_{\boldsymbol{X}} \frac{\mu}{2}\|\boldsymbol{Y} - \boldsymbol{F}\boldsymbol{X}\|_2^2 + TV(\boldsymbol{X}), \quad (7)$$

where, for example, $\|\boldsymbol{q}\|_2^2$ is the ℓ_2 norm (Euclidean norm) of $\boldsymbol{q}$ and μ is a constant. The first penalty is a least-squares term that is small when $\boldsymbol{X}$ is consistent with the correlation

vector $\boldsymbol{Y}$. The second penalty $TV(\boldsymbol{X})$ is the signal's total variation,

$$TV(\boldsymbol{X}) = \sum_{\text{adj.}i,j} |\boldsymbol{X}_i - \boldsymbol{X}_j|, \tag{8}$$

where indices i, j run over all pairs of adjacent pixels in $\boldsymbol{X}$ so that $TV(\boldsymbol{X})$ is just the ℓ_1 norm of $\boldsymbol{X}$'s discrete gradient.

If a signal's total variation is large, values of adjacent pixels vary wildly, indicating a noisy, unstructured signal. Conversely, when a signal's total variation is small, values for adjacent pixels are strongly correlated, indicating structure consistent with a real image. Put more plainly, we seek the signal with the fewest edges consistent with our measurements; this leverages compressibility in $\boldsymbol{X}$'s gradient. Total variation minimization has proven extremely effective for compressive imaging; exact recovery of $\boldsymbol{X}$ is possible with M as low as a few percent of N [26]. In addition to sub-Nyquist sampling, CS has been shown to give a higher signal-to-noise ratio than raster or basis scans [27].

We tested our technique on four objects: a double slit, a triple slit, the character $\hbar$, and the University of Rochester logo (Fig. 4). The object and filter masks were introduced using computer controlled spatial light modulators, which can change patterns at typical video speeds up to 60 Hz. The filter spatial resolution was $N = 256 \times 256$ pixels. The random filter functions were rows of a randomly permuted, zero-shifted Hadamard matrix [28]. This allows $\boldsymbol{Y} = \boldsymbol{F}\boldsymbol{X}$ to

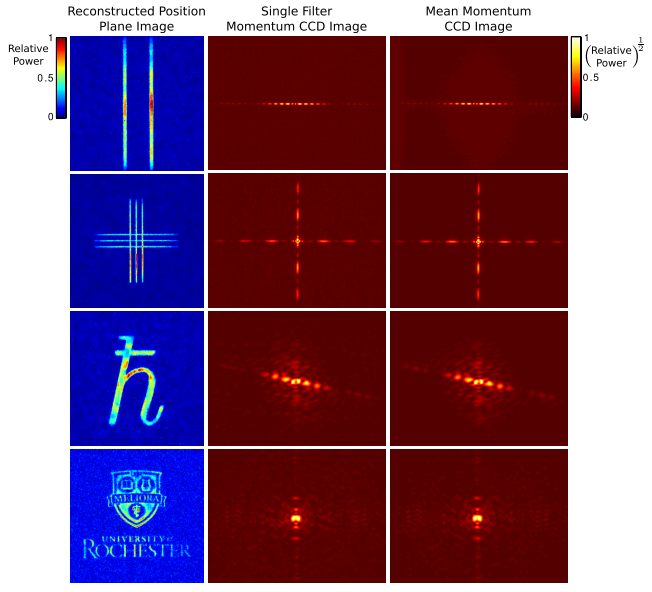

FIG. 4 (color online). Recovered position and momentum images for four objects. A double slit, triple slit, and $\hbar$ were reconstructed at $N = 256 \times 256$ resolution from only $M = 6553$ filters; the university logo used $M = 32768$ filters. No additional post-processing has been performed; position images are those returned by the reconstruction algorithm and momentum images are the recorded single or mean CCD images.

be efficiently computed by a fast transform when solving Eq. (7).

The CCD was a cooled, 12-bit, 1376×1040-pixel sensor. The exposure time for each CCD image was 10 ms. The average optical power incident on the CCD was of order 10 pW. For a 10 ms exposures, each CCD pixel had dark noise 50 ± 10 in arbitrary power units of 0 to 4096. When integrating the CCD image to produce the correlation vector $\boldsymbol{Y}$, this value was subtracted. Momentum images are those recorded directly by the camera; no post-processing is performed beyond averaging over all images.

For the double slit, triple slit, and character objects, $M = 0.1N = 6553$ filters were used; for the university logo, $M = 0.5N = 32768$ filters were used. These correspond to total exposure times of 65.5 sec and 327.7 sec, respectively. Note that Nyquist sampling would require N measurements; for most objects we undersample by an order of magnitude. The requisite M depends both on object complexity and the chosen objective function [Eq. (7)], sensing matrix, and solving algorithm. We have chosen a conservatively large M to produce high-quality images. The dependence of image quality on M is extensively researched; for example, see Refs. [14,15,27].

The position distributions were reconstructed by solving Eq. (7) using the TVAL3 solver [29]. Values of μ ranged from 2^{10} to 2^{14}. Such large μ strongly favors the least-squares penalty of Eq. (7) such that it is effectively a constraint.

In all cases, our technique recovered high-fidelity position and momentum distributions. Even momentum images for a single filter are good approximations to the true distribution; these are further improved by averaging.

To show the accuracy of our technique, Fig. 5 gives the mean-squared errors (MSEs) of the momentum images for 100 simulations of the objects used in the experiment as a function of increasing M. Even for a single pattern, the MSE is at least of order 10^{-7}. Averaging over an increasing number of patterns, the middle term of Eq. (4) vanishes and the MSE approaches a constant. This occurs within a few hundred patterns, well before the requisite M for recovering the position image.

We have demonstrated an efficient technique for measuring the probability distributions of complementary observables from a single set of measurements. Beyond fundamental interest, we anticipate that our approach will be useful for a wide variety of quantum and classical sensing tasks, including continuous quantum measurement [30], high-dimensional entanglement characterization [21], wave-front sensing, and phase retrieval [31]. We strongly emphasize that our technique does not violate the uncertainty principle; at no point does a single detection event give precise information about both position and momentum. Instead, each detection event gives some information about both domains. Our approach economizes the use of this information. More broadly, our system exemplifies a

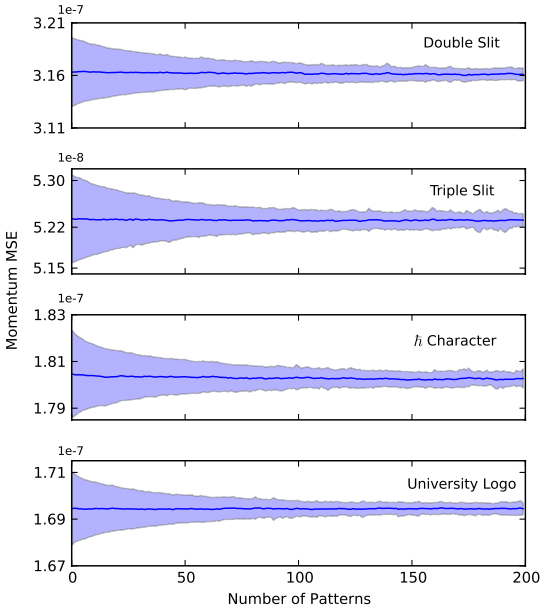

FIG. 5 (color online). Simulated momentum MSE: The simulated momentum MSEs of the four objects used in the experiment are given as a function of the number of random patterns M. The shaded region encloses one standard deviation above and below the average MSE for 100 trials. The MSE rapidly approaches a small constant value as the second term of Eq. (4) vanishes. Even for a single pattern, the MSE is at least of order 10^{-7}.

trend in sensing away from traditional strong projective measurements and raster scans which scale poorly to large dimensions. Novel techniques based on compressive sensing, weak measurement, and other unorthodox strategies are necessary to overcome these limitations.

This work was supported by AFOSR Grant No. FA9550-13-1-0019 and DARPA DSO InPho Grant No. W911NF-10-1-0404.

*ghowland@pas.rochester.edu

[1] N. Bohr, Nature (London) **121**, 580 (1928).
[2] B. C. Platt *et al.*, J. Refract. Surg. **17**, S573 (2001).
[3] H. Maassen and J. B. M. Uffink, Phys. Rev. Lett. **60**, 1103 (1988).
[4] M. J. W. Hall, Phys. Rev. Lett. **74**, 3307 (1995).
[5] J. S. Lundeen, B. Sutherland, A. Patel, C. Stewart, and C. Bamber, Nature (London) **474**, 188 (2011).
[6] S. Kocsis, B. Braverman, S. Ravets, M. J. Stevens, R. P. Mirin, L. K. Shalm, and A. M. Steinberg, Science **332**, 1170 (2011).
[7] J. Dressel, M. Malik, F. M. Miatto, A. N. Jordan, and R. W. Boyd, Rev. Mod. Phys. **86**, 307 (2014).
[8] D. L. Donoho, IEEE Trans. Inf. Theory **52**, 1289 (2006).
[9] J. W. Goodman, *Introduction to Fourier optics* (Roberts and Company Publishers Greenwood Village, CO, 2005).
[10] W. McCrea and F. Whipple, Proc. R. Soc. Edinburgh **60**, 281 (1940).
[11] See Supplemental Material http://link.aps.org/supplemental/10.1103/PhysRevLett.112.253602, for rigorous derivation of Eqs. (3) and (4), which includes Refs. [32–34].
[12] D. Tse, *Fundamentals of wireless communication* (Cambridge University Press, Cambridge, England, 2005).
[13] R. G. Baraniuk, IEEE Signal Process. Mag. **24**, 118 (2007).
[14] R. G. Baraniuk, IEEE Signal Process. Mag. **25**, 12 (2008).
[15] J. Romberg, IEEE Signal Process. Mag. **25**, 14 (2008).
[16] M. Lustig, D. Donoho, and J. M. Pauly, Magn. Reson. Med. **58**, 1182 (2007).
[17] J. Bobin, J.-L. Starck, and R. Ottensamer, IEEE Journal of Selected Topics in Signal Processing **25**, 2 (2008).
[18] D. Gross, Y.-K. Liu, S. T. Flammia, S. Becker, and J. Eisert, Phys. Rev. Lett. **105**, 150401 (2010).
[19] M. Cramer, M. B. Plenio, S. T. Flammia, R. Somma, D. Gross, S. D. Bartlett, O. Landon-Cardinal, D. Poulin, and Y.-K. Liu, Nat. Commun. **1**, 149 (2010).
[20] A. Shabani, R. L. Kosut, M. Mohseni, H. Rabitz, M. A. Broome, M. P. Almeida, A. Fedrizzi, and A. G. White, Phys. Rev. Lett. **106**, 100401 (2011).
[21] G. A. Howland and J. C. Howell, Phys. Rev. X **3**, 011013 (2013).
[22] B. Sun, M. P. Edgar, R. Bowman, L. E. Vittert, S. Welsh, A. Bowman, and M. Padgett, Science **340**, 844 (2013).
[23] O. Katz, Y. Bromberg, and Y. Silberberg, Appl. Phys. Lett. **95**, 131110 (2009).
[24] D. Takhar, J. N. Laska, M. B. Wakin, M. F. Duarte, D. Baron, S. Sarvotham, K. F. Kelly, and R. G. Baraniuk, in *Electronic Imaging 2006* (International Society for Optics and Photonics, Bellingham, WA, 2006), p. 606509.
[25] S. S. Welsh, M. P. Edgar, R. Bowman, P. Jonathan, B. Sun, and M. J. Padgett, Opt. Express **21**, 23068 (2013).
[26] E. J. Candes and T. Tao, IEEE Trans. Inf. Theory **52**, 5406 (2006).
[27] E. J. Candès and M. B. Wakin, IEEE Signal Process. Mag. **25**, 21 (2008).
[28] C. Li, Ph.D. thesis, Rice University, (2011).
[29] C. Li, W. Yin, and Y. Zhang, CAAM Report (2009).
[30] K. Jacobs and D. A. Steck, Contemp. Phys. **47**, 279 (2006).
[31] J. R. Fienup, Appl. Opt. **21**, 2758 (1982).
[32] E. J. Candès *et al.*, in *Proceedings of the International Congress of Mathematicians Madrid, Spain, August 22–30, 2006*, edited by M. Sanz-Solé, J. Soria, J. L. Varona, and J. Verdera (European Mathematical Society, Zurich, 2007), p. 1433.
[33] Y. Wang, J. Yang, W. Yin, and Y. Zhang, SIAM Journal on Imaging Sciences **1**, 248 (2008).
[34] E. J. Candès, J. Romberg, and T. Tao, IEEE Trans. Inf. Theory **52**, 489 (2006).